The valence state of Ce in electron-doped manganites: $La_{0.7}Ce_{0.3}MnO_3$

2001 J. Phys.: Condens. Matter 13 3779

(http://iopscience.iop.org/0953-8984/13/16/308)

INSTITUTE OF PHYSICS PUBLISHING JOURNAL OF PHYSICS: CONDENSED MATTER

J. Phys.: Condens. Matter **13** (2001) 3779–3789 www.iop.org/Journals/cm PII: S0953-8984(01)19857-7

The valence state of Ce in electron-doped manganites: $La_{0.7}Ce_{0.3}MnO_3$

J-S Kang[1], Y J Kim[2], B W Lee[2], C G Olson[3] and B I Min[4]

[1] Department of Physics, The Catholic University of Korea, Puchon 422-743, Korea
[2] Department of Physics, Hankuk University of Foreign Studies, Yongin, Kyungki 449-791, Korea
[3] Ames Laboratory, Iowa State University, Ames, IA 50011, USA
[4] Department of Physics, Pohang University of Science and Technology, Pohang 790-784, Korea

Received 7 December 2000, in final form 14 March 2001

Abstract

The electronic structure of $La_{0.7}Ce_{0.3}MnO_3$ (LCeMO) has been investigated by using photoemission spectroscopy. A very weak 4f resonance is observed and the Ce 3d spectrum of LCeMO is very similar to that of CeO_2, indicating that Ce ions are far from being trivalent. The Mn 2p core-level spectrum of LCeMO is essentially the same as that of hole-doped $La_{0.7}Sr_{0.3}MnO_3$, but different from that of MnO. The local spin-density approximation (LSDA) electronic structure calculations for LCeMO show that the Mn 3d states contribute a large peak around -2 eV and a weak structure between -2 eV and E_F, and that the O 2p states are spread between -3 eV and -9 eV, with negligible contribution near E_F. The LSDA calculations for LCeMO and hole-doped $La_{0.7}Ba_{0.3}MnO_3$ reveal that the calculated Mn 3d density of states at E_F in LCeMO is larger, reflecting the effect of electron doping with Ce ions.

1. Introduction

The discovery of the colossal-magnetoresistance (CMR) phenomenon in the perovskite Mn oxides of $R_{1-x}A_xMnO_3$ (RAMO; R: rare earth; A: divalent cation) has generated wide interest [1]. On the basis of correlations found in their phase diagrams, these systems are considered as spin–charge–lattice coupled systems. In a divalent-ion-doped RAMO system, Mn ions can exist in the formally trivalent and tetravalent states. Then the Zener-type double-exchange (DE) between spin-aligned Mn^{3+} ($t_{2g}^3e_g^1$) and Mn^{4+} (t_{2g}^3) ions through oxygen ions gives rise to metallic conductivity and ferromagnetism [2].

In the DE model, Mn ions should exist in a mixed-valence state to maintain the correlation between magnetism and conductivity. The question has been raised of whether the DE mechanism is still operative when a tetravalent ion is used for the doping instead of a divalent ion [3], causing an electron doping similarly to that in the high-T_C superconductor $Nd_{2-x}Ce_xCuO_y$ [4]. This will result in a system with a mixed-valence state of Mn^{2+} ($t_{2g}^3e_g^2$) and Mn^{3+} ($t_{2g}^3e_g^1$) ions. Interestingly, the metal–insulator (M–I) and ferromagnetic transitions and the concomitant CMR phenomenon have been observed in the Ce-doped manganites

$R_{0.7}Ce_{0.3}MnO_3$ (RCeMO; R = La, Pr, Nd) [3, 5]. If Ce ions in RCeMO exist in a tetravalent state, Mn^{2+} ions could be formed and electron-like charge carriers would be responsible for the metallic conductivity and ferromagnetism. Therefore it is essential to know the valence states of Ce and Mn ions to understand the nature of the charge carriers in RCeMO and the underlying physics properly.

Despite extensive photoemission spectroscopy (PES) studies on the manganites [6–13], no PES study on RCeMO has been reported yet. In this paper, we have explored the valence states of Ce and Mn ions in $La_{0.7}Ce_{0.3}MnO_3$ (LCeMO), using resonant photoemission spectroscopy (RPES) near the Ce 4d $\rightarrow$ 4f and Mn 3p $\rightarrow$ 3d absorption edges and x-ray photoemission spectroscopy (XPS) of the Ce 3d and Mn 2p core levels. Experimental results are compared to the band-structure calculations performed in the local spin-density approximation (LSDA).

2. Experimental and calculational details

Polycrystalline LCeMO samples were prepared by the conventional solid-state reaction methods, using high-purity (99.99% or better) La_2O_3, CeO_2, and Mn_2O_3 powders. The as-prepared LCeMO sample was annealed at 1050 °C in oxygen for five hours. The x-ray powder diffraction pattern for LCeMO showed a clean single-phase pattern similar to that in reference [3]. Resistivity and magnetization measurements for LCeMO showed behaviours very similar to those reported in references [3, 5], with a simultaneous M–I and ferromagnetic transition at temperature $T_R \sim 260$ K and the residual resistivity of $\rho_0 \sim 0.1\,\Omega$ cm at $T \leqslant 20$ K.

PES experiments were carried out at the Ames/Montana beam-line at the Synchrotron Radiation Center (SRC). Samples were fractured and measured in vacuum with a base pressure better than 4×10^{-11} Torr and at $T < 20$ K. The Fermi level E_F of the system was determined from the valence-band spectrum of a sputtered Pt foil. The total instrumental resolution (FWHM: full width at half-maximum) was about 90 meV at $h\nu = 22$ eV and 250 meV at $h\nu \sim 120$ eV. All the spectra were normalized to the mesh current. The cleanliness of the fractured surfaces was monitored using a hump around 9 eV binding energy (BE) in the valence-band spectrum obtained at a low photon energy. Figure 1 shows the valence-band energy distribution curves (EDCs) of LCeMO for 20 eV $\leqslant h\nu \leqslant$ 121 eV. At a low $h\nu \sim 26$ eV, a small and broad hump is observed around 10 eV BE, probably due to the CO (carbon monoxide) present on the surface. This feature is not observed at higher $h\nu$ because of the cross-section of this peak rapidly decreasing with $h\nu$. The intensity of the 10 eV hump is sufficiently low that the intrinsic valence-band features are still observed in our valence-band spectra. This will be further discussed in relation to figure 5, later.

Core-level spectra of LCeMO were obtained using a Perkin-Elmer PHI 5400 ESCA spectrometer equipped with a twin anode (Mg, Al). The base pressure of the system was about 2×10^{-10} Torr and the samples were scraped and measured at room temperature with an overall instrumental resolution of about 1 eV at the FWHM for Ag $3d_{5/2}$. The survey spectrum showed no contaminations except for a small carbon (C) 1s peak, corresponding to an estimated concentration of about 5–10%. This carbon seemed to be present in the bulk and to diffuse out from inside the bulk to the surface because the core-level XPS measurements were done at room temperature. The presence of the C 1s signal did not affect the line-shapes of other core levels of metallic elements, but caused a reduction in the overall intensity of other core levels[1]. The x-ray satellites due to the Mg $K\alpha_{3,4}$ radiation were subtracted.

[1] It is likely that this carbon is not involved in bonding and does not affect the intrinsic line-shapes of other core levels.

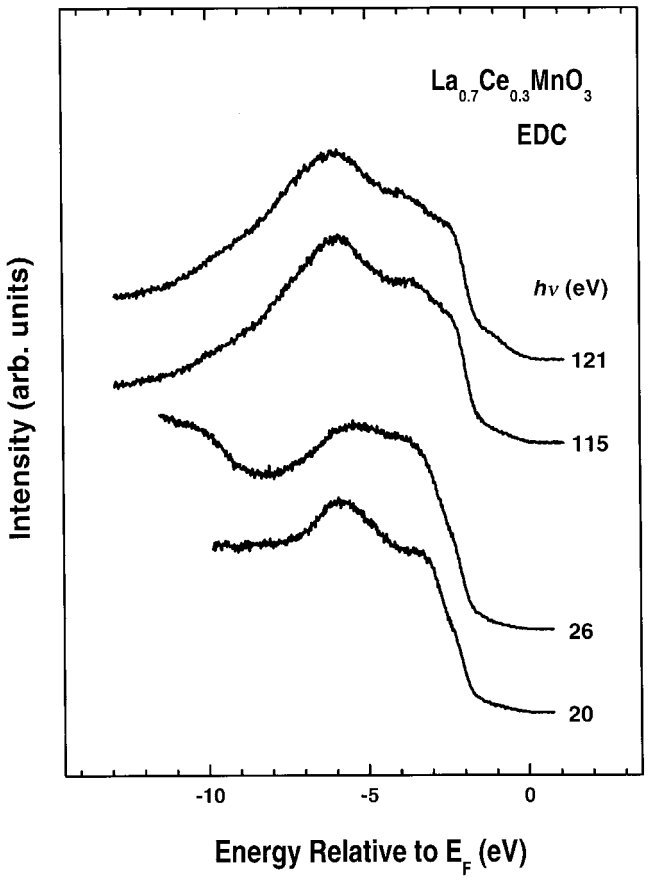

Figure 1. Energy distribution curves (EDCs) of LCeMO for 20 eV $\leqslant h\nu \leqslant$ 121 eV.

The electronic structures of LCeMO have been calculated by using density-functional calculations within the LSDA on the basis of the linearized muffin-tin orbital (LMTO) band method. The von Barth–Hedin form of the exchange–correlation potential was utilized. The angular-momentum-projected local densities of states (PLDOSs) for $La_{0.7}R_{0.3}MnO_3$ (R = Ba, Ce) were obtained from the LSDA band-structure calculations using the virtual-crystal approximation (VCA) [14]. Ferromagnetic phases of the cubic structure (lattice constant: 3.872 Å) are considered for both manganites $La_{0.7}R_{0.3}MnO_3$ (R = Ba, Ce).

3. Results and discussion

Figure 2 presents the normalized valence-band spectra for LCeMO with $h\nu = 121$ eV (on-resonance) and $h\nu = 115$ eV (off-resonance). As a comparison, those for $Pr_{0.3}Sr_{0.7}MnO_3$ with $h\nu = 124$ eV (on-resonance) and $h\nu = 119$ eV (off-resonance) are also presented, for which the Pr ions are known to be trivalent ($4f^2$) [13]. The off-resonance spectra have been scaled by a factor of 0.9 [15] for both LCeMO and $Pr_{0.3}Sr_{0.7}MnO_3$. This factor is roughly taken to account for the dependence on $h\nu$ of the non-4f emission. The difference of each pair, referenced to the off-resonance spectra, represents the R 4f resonance (R = Ce, Pr), and is expected to be a measure of the 4f occupancy.

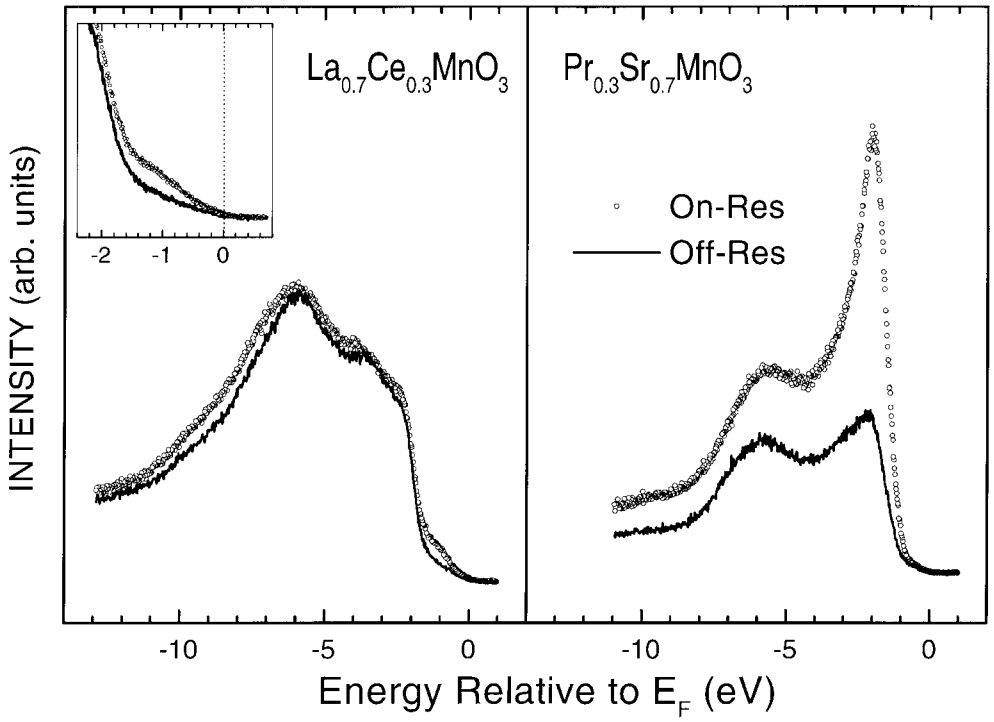

Figure 2. Left: normalized valence-band spectra for LCeMO, obtained at the 4f resonance (open circles) and at the off-resonance (solid lines). Right: similarly for $Pr_{0.3}Sr_{0.7}MnO_3$.

In contrast to the large 4f resonance in $Pr_{0.3}Sr_{0.7}MnO_3$, the magnitude of the 4f resonance in LCeMO is very weak. This feature indicates that the localized Ce 4f states are nearly unoccupied in LCeMO and that the Ce valence is far from 3+. This is because RPES for the R 4d absorption edge involves atomic processes of the type

$$4d^{10}4f^n + h\nu \rightarrow 4d^9 4f^{n+1} \rightarrow 4d^{10}4f^{n-1}\epsilon_k \tag{1}$$

where ϵ_k denotes the emitted electron. The first step is a photoabsorption of a 4d electron to an unoccupied 4f state, leading to an intermediate state. The second step is a two-electron Coster–Kronig decay of the intermediate state, involving an Auger matrix element of the Coulomb interaction $\langle 4d, \epsilon_k|(1/r_{12})|4f, 4f\rangle$. The same final state can also be reached by a direct photoemission process:

$$4d^{10}4f^n + h\nu \rightarrow 4d^{10}4f^{n-1}\epsilon_k. \tag{2}$$

The interference between these two processes leads to the so-called Fano resonance that depends on the details of the decay channels. For a tetravalent Ce^{4+} ion ($4f^0$), such a RPES process will not be invoked because $n - 1 < 0$. This finding is in fact consistent with that for the Ce 3d core-level XPS (see figure 4, later).

The inset of figure 2 shows the enlarged spectra near E_F. No metallic Fermi edge is observed in LCeMO at $T \sim 20$ K, well below T_R, probably due to the large residual resistivity of LCeMO. The Ce 4f contribution is the largest around 1 eV below E_F with no Ce 4f contribution at E_F. The Ce 4f spectral weight distribution in LCeMO is very weak and does not exhibit a double-peak structure, unlike those for other Ce compounds [16, 17].

Figure 3 compares the constant-initial-state (CIS) spectra of LCeMO for several initial-state energies E_i distributed through the valence bands, taken around the Ce 4d and Mn 3p absorption thresholds. In taking a CIS spectrum, $h\nu$ and E_K are simultaneously varied so as to keep $E_i = h\nu - \phi - E_K$ constant (E_K: kinetic energy; ϕ: work function). The CIS spectrum measures the RPES cross-section line-shape, determined by the initial and final states. For $h\nu \gtrsim 100$ eV, the CIS spectrum of LCeMO with $E_i = -1.0$ eV shows a very weak enhancement in the photoionization cross-section at around $h\nu \sim 121$ eV, corresponding to the Ce 4d $\rightarrow$ 4f absorption threshold [18]. It is difficult to tell whether its CIS line-shape is really a Fano line-shape because the enhancement is very weak, and yet this observation supports the finding in figure 2 that the electronic states at $E_i \sim -1.0$ eV certainly have the Ce 4f character. On the other hand, the CIS spectra with $E_i \leqslant -2.3$ eV reveal broad enhancement at about $h\nu \sim 117$ eV. In fact, this energy corresponds to the La 4d $\rightarrow$ 4f resonance energy required to induce the La 5d RPES via the Auger process with the Coulomb matrix element $\langle 4\mathrm{d}, \epsilon_k|(1/r_{12})|4\mathrm{f}, 5\mathrm{d}\rangle$ [19,20]. Hence, the broad enhancement for $E_i \leqslant -3.4$ eV has the La 5d electron character. This broad La 4d $\rightarrow$ 4f resonance for $h\nu$ around 115–120 eV overlaps with the very weak Ce 4d $\rightarrow$ 4f resonance in LCeMO. Therefore the resonant behaviour of the Ce 4f electron character in the valence-band region cannot be clarified for $E_i \lesssim -2$ eV.

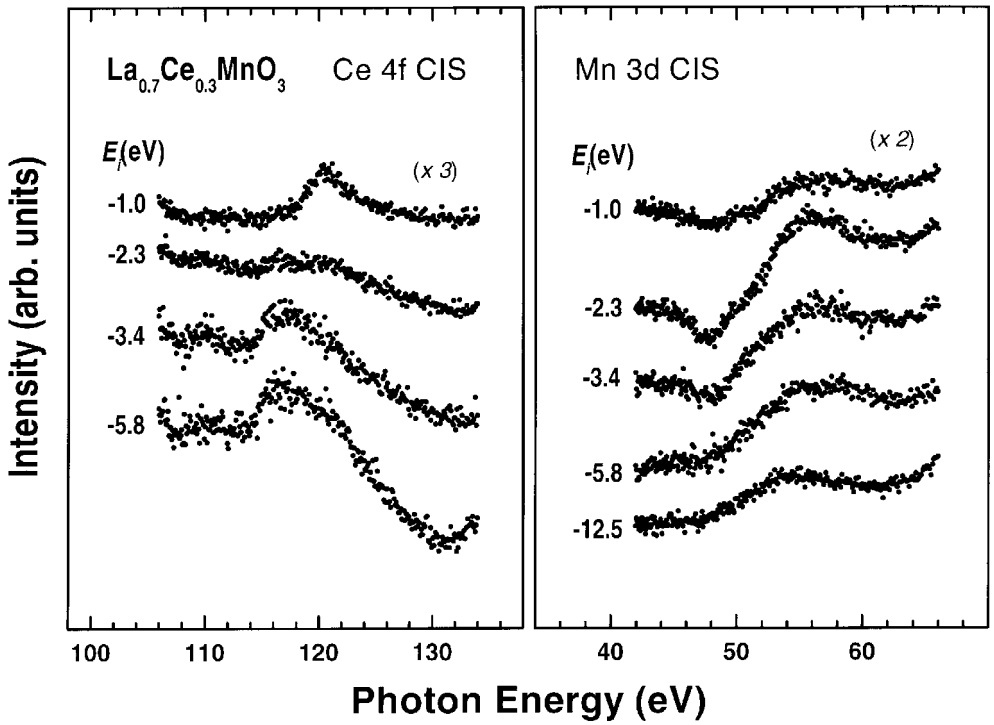

Figure 3. Constant-initial-state (CIS) spectra of LCeMO for several initial-state energies E_i, taken across the Ce 4d (left) and Mn 3p (right) absorption thresholds.

For $40 \lesssim h\nu \lesssim 70$ eV, the CIS spectra with $-6.0 \lesssim E_i \lesssim -1.0$ eV exhibit interference dips near the Mn 3p threshold ($h\nu \sim 48$ eV), as commonly observed in transition metals with unfilled 3d bands [21, 22]. This figure indicates that the Mn 3d states are spread over the whole valence band, i.e., the states with $-6.0 \lesssim E_i \lesssim -1.0$ eV have the Mn 3d electron

character. The Mn 3d contribution is the largest around −2.3 eV, consistent with the theoretical prediction in figure 5, later. However, the Mn 3p → 3d CIS spectra do not show any resonant enhancement that can be identified as an Mn 3d satellite [21].

Figure 4(a) compares the Ce 3d core-level spectra of LCeMO to those of the formally tetravalent CeO_2, the formally trivalent Ce_2O_3, and the nearly trivalent γ-Ce [18]. The 3d spectra of CeO_2, Ce_2O_3, and γ-Ce were reproduced from reference [23], reference [24], and reference [25], respectively. Each of the spin–orbit components of the 3d spectrum of LCeMO exhibits three peak structures. Of particular interest is the fact that the 3d spectrum of LCeMO is very similar to that of CeO_2, but quite different from those of Ce_2O_3 and γ-Ce. The highest BE peak for CeO_2, which is absent for Ce_2O_3, is known to have rather pure $3d^9f^0$ character. Thus the large intensities of the highest BE peaks for both LCeMO and CeO_2, in contrast to Ce_2O_3, account for the important f^0 character of their initial states. According to the impurity Anderson Hamiltonian analysis of the 3d core-level spectrum of CeO_2 [23], the two lower BE peaks are formed from a strong mixing of $3d^9f^1$ and $3d^9f^2$ final-state configurations with a ratio of the order of one. The localized 4f states remain completely unoccupied in CeO_2, but the valence-band states contain non-negligible extended states of f symmetry, responsible for the initial 4f population of $n_f \sim 0.5$.

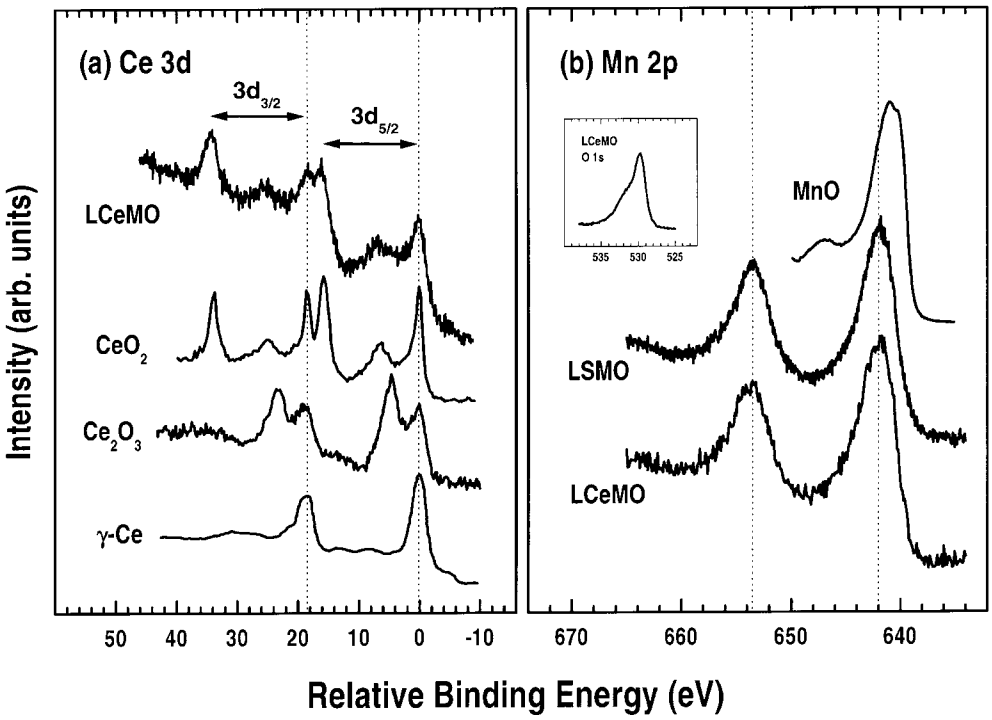

Figure 4. (a) The Ce 3d core-level spectrum of LCeMO, compared to those of CeO_2 (from reference [23]), Ce_2O_3 (from reference [24]), and γ-Ce (from reference [25]). (b) The Mn 2p core-level spectrum of LCeMO, compared to those of LSMO and MnO (from reference [26]). Inset: the O 1s core-level spectrum of LCeMO.

On the basis of the observation that the relative intensities of the three peaks for LCeMO are similar to those for CeO_2, one can conclude that the localized Ce 4f states are nearly unoccupied in LCeMO, which is consistent with a very weak Ce 4f resonance in figure 2. In general, it

is not possible to separate experimentally the Ce 4f occupancy into that of the localized 4f states and that of the valence-band states with f symmetry. Further, the concepts of valency and ionicity are not well defined, especially in the systems with the covalent bonding nature. In any case, our data provide evidence that the Ce valence is far from 3+, and accordingly suggest that the valence configurations of Mn ions in LCeMO are very different from those in RAMO.

Now we address the question of the valence state of Mn. If the electrons doped in via the Ce substitution go to the Mn e_g bands, Mn ions have mixed-valence states that are combinations of Mn^{2+} and Mn^{3+}. In figure 4(b), the Mn 2p core-level spectrum of LCeMO is compared to those of hole-doped $La_{0.7}Sr_{0.3}MnO_3$ (LSMO) with formally mixed-valence Mn^{3+}/Mn^{4+} ions, and also MnO with a formal Mn valence of 2+. The latter spectrum is reproduced from reference [26]. The Mn 2p spectrum of LCeMO is essentially the same as that of LSMO within the experimental resolution, but rather different from that of MnO, which shows a satellite structure at about 6 eV higher BE. This comparison may indicate that Mn^{2+} ions are not likely to be formed in LCeMO. On the other hand, the multiplet splitting for the Mn^{3+} final-state configurations ($2p^5 3d^4\underline{L}^0$, $2p^5 3d^5\underline{L}^1$, $2p^5 3d^6\underline{L}^2$; where $\underline{L}$ denotes a ligand hole) is rather large ($\sim$5 eV) [7], compared to the energy difference between the 2p core levels of the Mn^{3+} and Mn^{2+} ions. Thus the similarity of the measured Mn 2p spectra of LCeMO and LSMO is not necessarily to be taken to indicate similar Mn 3d electronic structures of LCeMO and LSMO. The O 1s core-level spectrum of LCeMO is shown in the inset of figure 4(b); it reveals a single peak with a rather asymmetric line-shape on the high-BE side of $\sim$531 eV, probably due to the emission from some adsorbed water on the surface or defects at the grain boundaries. The O 1s spectrum of LSMO (not shown here) is similar to that of LCeMO.

To help to explain the microscopic origin of the valence-band electronic structures of LCeMO, the calculated LSDA electronic structures of LCeMO are shown in figure 5. The upper and lower curves in the upper two panels represent the majority-spin and minority-spin O 2p PLDOS, and the majority-spin and minority-spin Mn 3d PLDOS, respectively. The bottom panel compares the O 2p (dots) and Mn 3d PLDOS (solid line). The peak positions and the intensity distributions of the O 2p and Mn 3d PLDOSs reflect the large hybridization between the Mn d and O p states. Most of the O 2p PLDOS is located between -3 eV and -9 eV, and its contribution near E_F is negligible. These predictions are consistent with the features observed in the valence-band spectrum at $h\nu \sim 20$ eV (figure 1). Note that the three salient large-energy structures in the calculated O 2p PLDOS (at around -2 eV, -4 eV, and -7 eV) are also consistent with those in the measured valence-band spectrum at $h\nu \sim 20$ eV in figure 1. A small peak is observed around -2 eV due to the majority-spin O 2p states, reflecting the effect of the hybridization to the majority-spin Mn t_{2g} states. The Mn 3d PLDOS shows a large peak around -2 eV due to the majority-spin Mn t_{2g} states. The calculated exchange splitting is about 3 eV. The LSDA calculations yield the metallic ground state for LCeMO, and the Fermi level cuts the middle of the Mn $e_g^{\uparrow}$ band and the bottom of the Mn $t_{2g}^{\downarrow}$ band. The calculated O 2p and Mn 3d PLDOSs suggest that the peak around -2 eV in the measured photoemission spectra is mainly due to the Mn t_{2g} emission.

In order to examine the differences in Mn 3d electronic state between LCeMO and another hole-doped RAMO compound, we have compared the calculated Mn 3d PLDOSs for two typical systems, one being hole-doped $La_{0.7}Ba_{0.3}MnO_3$ (LBaMO) and the other being electron-doped LCeMO, in figure 6. The calculated electronic structure of LBaMO reveals a half-metallic ground state, consistent with the prediction for another hole-doped RAMO compound [27], and the Mn 3d PLDOS of LBaMO is very similar to that of hole-doped PSMO [13]. Even though the overall features in the Mn 3d PLDOSs of LBaMO and LCeMO are similar to each other, the peak positions in LCeMO are shifted to higher BEs compared to

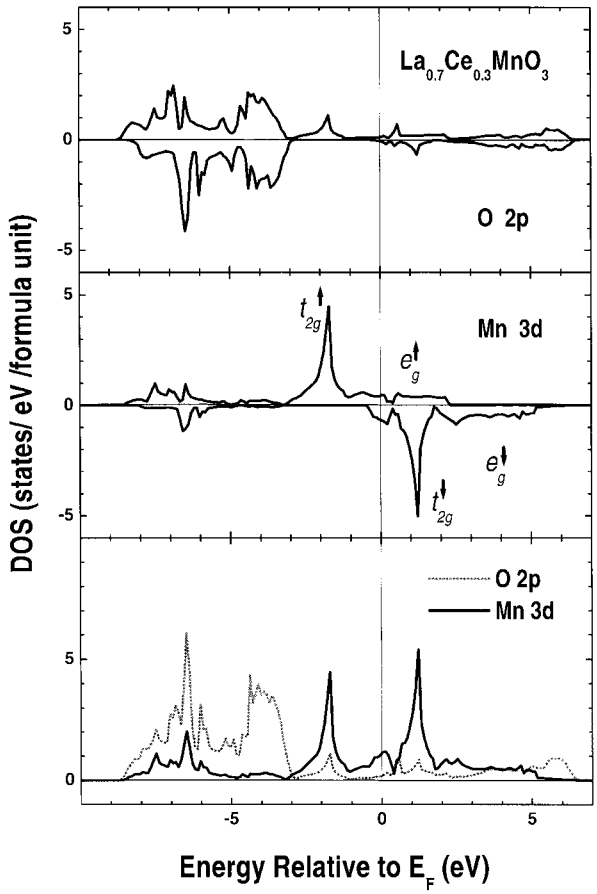

Figure 5. The calculated projected local density of states (PLDOS) for LCeMO. From the top, the majority-spin (upper curve) and minority-spin (lower curve) O 2p PLDOS, the majority-spin (upper curve) and minority-spin (lower curve) Mn 3d PLDOS, and the comparison of the O 2p PLDOS (dots) and the Mn 3d PLDOS (solid line).

those for LBaMO. Such systematic changes arise from the rigid shift of E_F toward a higher energy that occurs in LCeMO because of extra doped electrons, resulting in a normal metal with a larger Mn 3d PLDOS at E_F.

Note that the off-resonance spectrum of LCeMO (figure 2) reveals a very weak spectral intensity between -1 eV and E_F. In combination with the negligible O 2p PLDOS at E_F (figure 5), this finding suggests that the Mn 3d spectral intensity near E_F is very low in LCeMO. It is difficult to separate out the Mn 3d partial spectral weight (PSW) distribution from the O 2p PSW using our data because the O 2p emission is dominant for $h\nu \lesssim 120$ eV. According to reference [15], the estimated O 2p and Mn 3d emissions in LCeMO are as follows: O 2p:Mn 3d $= \sim$60%:$\sim$40% at $h\nu \sim 120$ eV, and $\sim$85%:$\lesssim$10% at $h\nu \sim 20$ eV. Further, the O 2p and Mn 3d states are strongly mixed in the manganites, as shown in figure 5 and other works [7–9, 11–13, 28].

The finding of the low Mn 3d spectral intensity near E_F for LCeMO contrasts with the calculated Mn 3d PLDOS between E_F and -2 eV (figure 6). There are several possibilities for the cause of the discrepancy between theory and experiment.

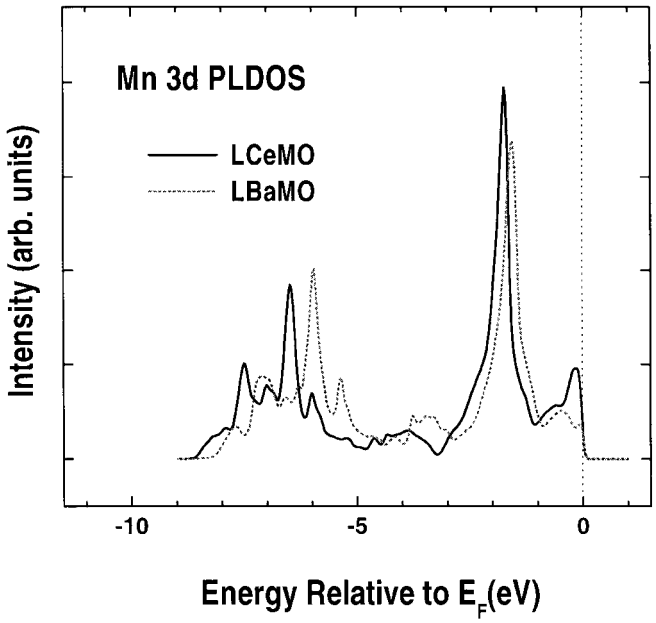

Figure 6. Comparison of the calculated Mn 3d PLDOSs of LCeMO and LBaMO.

(i) The photon energy range employed in this work is rather surface sensitive [12, 16, 17], and the surface spectral weight near E_F might be smaller than the bulk spectral weight. A more bulk-sensitive PES measurement, such as Mn 2p $\rightarrow$ 3d RPES, would be helpful for obtaining the bulk Mn 3d spectral weight [9, 12].

(ii) A carrier localization mechanism in LCeMO would reduce the spectral intensity close to E_F yielding a pseudogap, which is probably due to the strong e_g electron–phonon interaction originating from the Jahn–Teller-active Mn ions as in other hole-doped manganites [11].

(iii) A possible additional localization mechanism in LCeMO is the large Coulomb correlation interaction U_{eff} between Mn e_g electrons. Provided that doped electrons are transferred to Mn ions, these electrons will sit on the upper empty e_g band and change Mn^{3+} ions into Mn^{2+} ions. This change induces a large Coulomb interaction ($U_{eff} \gtrsim 3$ eV [9]) between Mn e_g electrons and so plays the role of reducing the spectral intensity near E_F. Indeed the LSDA + U electronic structure calculation for LCeMO incorporating the Coulomb correlation parameter U yields the result that the PLDOS near E_F is much suppressed as compared to that in the LSDA [29]. Furthermore, the separation between the two t_{2g} majority- and minority-spin bands becomes larger in the LSDA + U calculation, leading to a half-metallic nature for LCeMO.

(iv) Finally, the extended Ce 4f states will cause a substantial redistribution of the quasi-particle weight via the hybridization interaction with the Mn 3d electrons.

It is noteworthy that the transport behaviour of LCeMO is very sensitive to the growth condition that influences the oxygen content in LCeMO. Then, even if Ce ions in LCeMO exist in tetravalent states, excess oxygens, if they exist, will compensate for electrons doped in by Ce ions to reduce the amount of formal Mn^{2+} ions. Indeed a recent transport study of LCeMO films indicates that T_R decreases and resistivity increases with increasing oxygen pressure [30]. Mn NMR experiments for LCeMO also indicate the content of Mn^{2+} ions to

be minor with excess oxygens [31], implying that excess oxygens in LCeMO compensate for doped electrons, and so lower the content of the Mn^{2+} ions. Therefore, for the determination of the correct valence states of Mn ions, it is prerequisite to know the content of excess oxygen in LCeMO precisely. Unfortunately, the determination of the amount of the oxygen is not trivial, and only recently have systematic investigations exploring the effects of the oxygen stoichiometry in hole- and electron-doped manganites been reported [30, 32].

The surface compositions are evaluated from our XPS data, and the estimated ratios of concentrations are as follows: La:Ce:Mn:O $\sim$ 0.72:0.28:0.93:3.5 for LCeMO, compared to La:Mn:O $\sim$ 1.0:0.83:3.4 for undoped $LaMnO_3$ (LMO) and La:Sr:Mn:O $\sim$ 0.75:0.25:0.89:3.4 for hole-doped LSMO[2]. These concentration ratios suggest that the excess oxygens are present in all of our perovskite samples. On the other hand, with respect to that of the undoped LMO sample, the oxygen content is roughly constant upon doping, suggesting that the doped holes or electrons would go to Mn sites. LCeMO shows a slightly higher oxygen content than in LMO or LSMO, implying that the excess oxygens in LCeMO might be the reason for the Mn 2p core-level spectra being the same for LCeMO and LSMO, and for the large 6 eV intensity in the valence-band spectrum of LCeMO. However, it is difficult to estimate the oxygen content precisely using the XPS data. According to our experience in XPS for other polycrystalline oxide and sulphide samples, the estimated concentrations of metallic elements are usually found to agree with the nominal compositions within about $\pm 5\%$ errors for the samples that show good physical properties. On the other hand, the concentration of the oxygen or sulphur element is often found to be substantially away from the nominal values even for the samples that show very good physical properties. Therefore in order to determine the Mn 3d electronic structure of LCeMO, it is important to carry out systematic high-resolution PES measurements on single crystals of both hole- and electron-doped systems with well-known oxygen stoichiometry.

4. Conclusions

We have performed RPES and Ce 3d and Mn 2p core-level XPS measurements for LCeMO, and calculated the Mn 3d PLDOSs of LBaMO and LCeMO using the LSDA and VCA approximations. A very weak Ce 4f resonance has been observed, indicating that the localized Ce 4f states are nearly unoccupied. The Ce 3d core-level spectrum of LCeMO is very similar to that of the formally tetravalent CeO_2, but different from that of the formally trivalent Ce_2O_3, implying that the Ce valence is far from 3+. The Mn 2p spectrum of LCeMO is very similar to that of LSMO, but different from that of MnO, implying that the content of Mn^{2+} ions is minor in the LCeMO sample that we used. The calculated PLDOSs for LCeMO show a large hybridization between the Mn 3d and O 2p states. Most of the O 2p PLDOS is located between -3 eV and -9 eV, with negligible contribution near E_F. The Mn 3d PLDOS has a large peak around -2 eV due to the majority-spin Mn t_{2g} states, and a weak structure close to E_F due to both the majority-spin Mn e_g and minority-spin Mn t_{2g} states. The calculated Mn 3d PLDOSs of LBaMO and LCeMO reveal similar overall features, but a larger Mn 3d PLDOS at E_F in LCeMO than in LBaMO, which is due to the electron doping with Ce ions. To determine the correct valence states of Mn ions in LCeMO, a precise study on the oxygen content is required.

[2] These concentration values are not to be taken seriously because the atomic photoionization cross-sections have been used and the transmission function of the analyser has been neglected in estimating the concentrations.

Acknowledgments

We thank S Lee for providing his NMR data before publication. This work was supported by the Centre for Strongly Correlated Materials Research at SNU, the KRF (2000-015-DP0116), the KOSEF (97-07-02-04-01-5), and the electron Spin Science Centre at POSTECH. The Synchrotron Radiation Center is supported by NSF (DMR-95-31009).

References

[1] Jin S, Tiefel T H, McCormack M, Fastnacht R A, Ramesh R and Chen L H 1994 *Science* **264** 413
[2] Zener C 1951 *Phys. Rev.* **82** 403
[3] Das S and Mandal P 1997 *Z. Phys.* B **104** 7
Mandal P and Das S 1997 *Phys. Rev.* B **56** 15 073
[4] Tokura Y, Takagi H and Uchida S 1989 *Nature* **337** 345
[5] Gebhardt J R, Roy S and Ali N 1999 *J. Appl. Phys.* **85** 5390
[6] Chainani A, Mathew M and Sarma D D 1993 *Phys. Rev.* B **47** 15 397
Chainani A, Kumigashira H, Takahashi T, Tomioka Y, Kuwahara H and Tokura Y 1997 *Phys. Rev.* B **56** R15 513
[7] Saitoh T, Bocquet A E, Mizokawa T, Namatame H, Fujimori A, Abbate M, Takeda Y and Takano M 1995 *Phys. Rev.* B **51** 13 942
[8] Sarma D D, Shanthi N, Krishnakumar S R, Saitoh T, Mizokawa T, Sekiyama A, Kobayashi K, Fujimori A, Takeda Y and Takano M 1996 *Phys. Rev.* B **53** 6873
[9] Park J-H, Chen C T, Cheong S-W, Bao W, Meigs F, Chakarian V and Idzerda Y U 1996 *Phys. Rev. Lett.* **76** 4215
[10] Park J-H, Vescovo E, Kim H-J, Kwon C, Ramesh R and Venkatesan T 1998 *Nature* **392** 794
[11] Dessau D S, Saitoh T, Park C-H, Shen Z-X, Villella P, Hamada N, Moritomo Y and Tokura Y 1998 *Phys. Rev. Lett.* **81** 192
[12] Sekiyama A, Suga S, Fujikawa M, Imada S, Iwasaki T, Matsuda K, Kaznacheyev K V, Fujimori A, Kuwahara H and Tokura Y 1999 *Phys. Rev.* B **59** 15 528
[13] Kang J-S, Olson C G, Jung J H, Lee H J, Noh T W and Min B I 1999 *Phys. Rev.* B **60** 13 257
[14] Youn S J and Min B I 1997 *Phys. Rev.* B **56** 12 046
[15] Yeh J J and Lindau I 1985 *At. Data Nucl. Data Tables* **32** 1
The photoionization cross-sections in actual solids are different from the atomic photoionization cross-sections.
[16] Duo L 1998 *Surf. Sci. Rep.* **32** 235
See the references therein. The bulk 4f spectrum could be somewhat different because of the surface contribution in the Ce 4d $\rightarrow$ 4f RPES being larger than that in the Ce 3d $\rightarrow$ 4f RPES, which is more bulk sensitive.
[17] Sekiyama A, Iwasaki T, Matsuda K, Saitoh Y, Onuki Y and Suga S 2000 *Nature* **403** 398
[18] Gerken F, Flodstrom A S, Barth J, Johansson L I and Kunz C 1985 *Phys. Scr.* **32** 43
[19] Lawrence J M, Allen J W, Oh S-J and Lindau I 1982 *Phys. Rev.* B **26** 2362
[20] Olson C G, Benning P J, Schmidt M, Lynch D W, Canfield P and Wieliczka D M 1996 *Phys. Rev. Lett.* **76** 4265
[21] Davis L C and Feldkamp L A 1981 *Phys. Rev.* B **24** 1862
In contrast to the interference dip observed for the main 3d band, the 3d satellites generally show resonant enhancement in the 3p $\rightarrow$ 3d resonance.
[22] Oh S-J, Allen J W, Lindau I and Mikkelsen J C Jr 1982 *Phys. Rev.* B **26** 4845
[23] Wuilloud E, Delley B, Schneider W-D and Baer Y 1984 *Phys. Rev. Lett.* **53** 202
[24] Allen J W 1985 *J. Magn. Magn. Mater.* **47+48** 168
[25] Fuggle J C, Hillebrecht F U, Zolnierek Z, Lässer R, Freiburg Ch, Gunnarsson O and Schönhammer K 1983 *Phys. Rev.* B **27** 7330
[26] van Elp J, Potze R H, Eskes H, Berger R and Sawatzky G A 1991 *Phys. Rev.* B **44** 1530
[27] Pickett W E and Singh D 1996 *Phys. Rev.* B **53** 1146
[28] Sarma D D, Shanthi N, Barman S R, Hamada N, Sawada H and Terakura K 1995 *Phys. Rev. Lett.* **75** 1126
[29] Min B I, Kwon S K, Lee B W and Kang J-S 2001 *J. Electron Spectrosc. Relat. Phenom.* **114–6** 801
[30] Raychaudhuri P, Mukherjee S, Nigam A K, John J, Vaisnav U D, Pinto R and Mandal P 1999 *J. Appl. Phys.* **86** 5718
[31] Dho J and Lee S 2000 private communications
[32] Krishnan K M and Ju H L 1999 *Phys. Rev.* B **60** 14 793